Journal of South American Earth Sciences 26 (2008) 355–368

Contents lists available at ScienceDirect

Journal of South American Earth Sciences

journal homepage: www.elsevier.com/locate/jsames

The contribution of the young Cretaceous Caribbean Oceanic Plateau to the genesis of late Cretaceous arc magmatism in the Cordillera Occidental of Ecuador

J. Allibon [a,b,*], P. Monjoie [b], H. Lapierre [1], E. Jaillard [b,c], F. Bussy [a], D. Bosch [d], F. Senebier [b]

[a] Institut de Minéralogie et de Géochimie, Anthropole, University of Lausanne, CH1015, Lausanne, Switzerland
[b] Laboratoire de Géodynamique des Chaînes Alpines, UMR 5025, Maison des Géosciences, 1381 rue de la piscine, 38400 Saint Martin d'Hères, France
[c] IRD-LMTG, Observatoire Midi-Pyrénées, 14 av. Edouard Belin, F31400, Toulouse, France
[d] Lab. Tectonophysique, UMR-CNRS 5568, cc049 Université Montpellier II, Pl. E. Bataillon, 34095 Montpellier Cedex 5, France

ARTICLE INFO

Article history:
Received 20 June 2007
Accepted 5 June 2008

Keywords:
Ecuador
Cretaceous island arcs
Oceanic plateau
Geochemistry
Isotopes
Modelling

ABSTRACT

The eastern part of the Cordillera Occidental of Ecuador comprises thick buoyant oceanic plateaus associated with island-arc tholeiites and subduction-related calc-alkaline series, accreted to the Ecuadorian Continental Margin from Late Cretaceous to Eocene times. One of these plateau sequences, the Guaranda Oceanic Plateau is considered as remnant of the Caribbean–Colombian Oceanic Province (CCOP) accreted to the Ecuadorian Margin in the Maastrichtien.

Samples studied in this paper were taken from four cross-sections through two arc-sequences in the northern part of the Cordillera Occidental of Ecuador, dated as (Río Cala) or ascribed to (Macuchi) the Late Cretaceous and one arc-like sequence in the Chogòn-Colonche Cordillera (Las Orquídeas). These three island-arcs can clearly be identified and rest conformably on the CCOP.

In all four localities, basalts with abundant large clinopyroxene phenocrysts can be found, mimicking a picritic or ankaramitic facies. This mineralogical particularity, although not uncommon in island arc lavas, hints at a contribution of the CCOP in the genesis of these island arc rocks.

The complete petrological and geochemical study of these rocks reveals that some have a primitive island-arc nature (MgO values range from 6 to 11 wt.%). Studied samples display marked Nb, Ta and Ti negative anomalies relative to the adjacent elements in the spidergrams characteristic of subduction-related magmatism. These rocks are LREE-enriched and their clinopyroxenes show a tholeiitic affinity (FeO_T–TiO_2 enrichment and CaO depletion from core to rim within a single crystal).

The four sampled cross-sections through the island-arc sequences display homogeneous initial Nd, and Pb isotope ratios that suggest a unique mantellic source for these rocks resulting from the mixing of three components: an East-Pacific MORB end-member, an enriched pelagic sediment component, and a HIMU component carried by the CCOP. Indeed, the ankaramite and Mg-basalt sequences that form part of the Caribbean-Colombian Oceanic Plateau are radiogenically enriched in $^{206}Pb/^{204}Pb$ and $^{207}Pb/^{204}Pb$ and contain a HIMU component similar to that observed in the Gorgona basalts and Galápagos lavas. The subduction zone that generated the Late Cretaceous arcs occurred far from the continental margin, in an oceanic environment. This implies that no terrigenous detrital sediments interacted with the source at this period. Thus, the enriched component can only result from the melting of subducted pelagic sediments.

We have thus defined the East-Pacific MORB, enriched (cherts, pelagic sediments) and HIMU components in an attempt to constrain and model the genesis of the studied island-arc magmatism, using a compilation of carefully selected isotopic data from literature according to rock age and paleogeographic location at the time of arc edification.

Tripolar mixing models reveal that proportions of 12–15 wt.% of the HIMU component, 7–15 wt.% of the pelagic sediment end-member and 70–75 wt.% of an East-pacific MORB end-member are needed to explain the measured isotope ratios. These surprisingly high proportions of the HIMU/CCOP component could be explained by the young age of the oceanic plateau (5–15 Ma) during the Late Cretaceous arc emplacement. The CCOP, basement of these arc sequences, was probably still hot and easily assimilated at the island-arc lava source.

1. Introduction

Examples of magmatism related to the subduction of oceanic lithosphere below an oceanic plateau are rare. Such a geodynamic

* Corresponding author. Address: Institut de Minéralogie et de Géochimie, Anthropole, University of Lausanne, CH1015, Lausanne, Switzerland. Fax: +41 21 692 43 05.
E-mail address: james.allibon@unil.ch (J. Allibon).
[1] Deceased January 14 2006.

0895-9811/$ - see front matter © 2008 Elsevier Ltd. All rights reserved.
doi:10.1016/j.jsames.2008.06.003

rarity can be illustrated by the Plio-Quaternary arc of the Solomon Islands caused by the subduction of the young and hot Woodlark Basin below the Cretaceous Ontong Java Oceanic Plateau and accreted to the Vityaz Arc 10 Ma ago (Ramsay et al., 1984; Petterson et al., 1997, 1999; Yoneshima et al., 2005; Gardien et al., 2008). Another example is the Late Cretaceous to Paleogene arcs established on the Caribbean–Colombian Oceanic Plateau (CCOP, 92–88 Ma, Sinton et al., 1998) accreted to the Ecuadorian margin from Campanian to Paleogene times (≈75–58 Ma).

In both cases, the generated basalts have very peculiar geochemical and petrological attributes marked by the existence of facies bearing large clinopyroxene phenocrysts as described by Ramsay et al. (1984) in the Solomon arc picrites. In the case of Ecuador, no arc-picrites were described, yet differentiated facies without olivine are found in association to olivine-bearing basalts that contain large centimetric diopside phenocrysts.

Geochemical studies of four cross-sections through three island arc sequences in Ecuador have been undertaken by Lebras et al. (1987), Reynaud et al. (1999), Hauff et al. (2000), Lapierre et al. (2000), Kerr et al. (2002), Mamberti et al. (2003, 2004), Chiaradia and Fontboté (2001, 2002), Chiaradia et al. (2004a,b), Luzieux et al. (2006) and Vallejo et al. (2006) and constrain the different volcanic phases between Cretaceous and Eocene times.

This subduction-related arc magmatism (as shown by the negative Nb, Ta, Zr and Ti anomalies relative to the adjacent elements in spidergrams) has very distinct attributes: The high proportions of olivine and clinopyroxene and the high MgO contents of these rocks suggest a high percentage of partial melting at the magmatic source. However the LREE enrichment implies either low percentages of partial melting- which is unlikely considering the high MgO values or an enriched source.

The origin of LREE enrichment of the Mg-rich basalts can be found in the involvement of subducted pelagic sediments as suggested by Ramsay et al. (1984) in their study of the Solomon Islands and by Mamberti et al. (2003) in their study of Ecuador.

If we consider that picrite or Mg-basalt genesis implies an anomalous heat source, then in the case of Ecuador such heat could be inherited from the young and residually hot CCOP. Indeed, these arc sequences established themselves in Campanian-Maastrichtian times (75–80 Ma) on a young (Vallejo et al., 2006) and therefore probably still hot oceanic plateau emplaced at 92–88 Ma (Sinton et al., 1998; Mamberti et al., 2003).

Chiaradia and Fontboté (2001, 2002) and Vallejo et al. (2006), suggest that a possible HIMU (plateau) component could be needed to explain whole-rock chemistry of the Macuchi island arc and of recent Quaternary volcanics. Similarly Mamberti et al. (2003) suggest possible contamination of the Río Cala island-arc magmatic rocks by the underlying oceanic plateau.

This paper focuses on the interactions between the CCOP and the overlying island-arc magmatism and attempts to model the extent of Oceanic Plateau contribution in the genesis of the island arc magmatism.

2. Geological setting

The Andes result from the eastward subduction of the paleopacific (Farallón) oceanic plate beneath the continental margin of western South America. The geological history of the Ecuadorian margin, however, differs from the rest of the central Andes. Due to a change in the Farallón plate convergence direction from SE to NE, the NNE-trending Ecuadorian margin evolved from an active margin in to a mainly transform margin around the Jurassic–Cretaceous boundary. This trend continued through Cretaceous times and allowed an Oceanic Plateau to develop offshore of Ecuador without interacting immediately with the margin. Plateau sequences support Cretaceous arc volcanism (Fig. 1) and accreted to the South American margin between Late Cretaceous and Paleogene times (Feininger and Bristow, 1980; Lebras et al., 1987; Reynaud et al., 1999; Mamberti et al., 2003; Jaillard et al., 2004, in press; Chiaradia et al., 2004a,b; Vallejo et al., 2006; Luzieux et al., 2006; Kerr and Tarney, 2005; Kerr and Mahoney, 2007).

Existing geochemical data concerning terranes of oceanic affinity reveal the existence of three possible distinct oceanic plateau sequences (Lebras et al., 1987; Reynaud et al., 1999; Lapierre et al., 2000; Mamberti et al., 2003, 2004; Kerr et al., 2002; Kerr and Tarney, 2005). The oldest, the San Juan oceanic plateau, is thought to be 123 Ma-old and accreted to the margin 75 Ma ago (Late Campanian, Lapierre et al., 2000; Jaillard et al., 2008), its existence is debated by many authors who suggest an age of 88.1 ± 1.6 Ma (Kerr and Tarney, 2005; Luzieux et al., 2006). The second oceanic plateau, the Guaranda plateau, is interpreted as part of the Caribbean–Colombian Oceanic Plateau (CCOP, Kerr et al., 1997a,b; Reynaud et al., 1999), dated to 92–88 Ma (Turonian–Coniacian, Sinton et al., 1998), and its age of accretion is said to be 68 Ma (Mid Maastrichtian, Jaillard et al., 2004). The Guaranda Plateau includes the Piñon Formation and probably the basement of northwestern coastal Ecuador (Fig. 1). Finally, a third oceanic plateau sequence, the Gorgona plateau (Kerr and Tarney, 2005) is said to be contemporaneous to the CCOP and accreted to the South American margin in Eocene times. The CCOP outcrops can be found in the Cordillera Occidental of Ecuador (Guaranda sequence, Mamberti et al., 2003) as well as in the coastal area between Guayaquil and Pedernales (Piñon fm., Reynaud et al., 1999; Luzieux et al., 2006). The Caribbean plateau is identified as picrite, ankaramite and basalt sequences crosscut by dolerite dykes (Mamberti et al., 2003) and overlain by radiolaritic limestones and cherts of Santonian age (Jaillard et al., 2004; Vanmelle et al., in press).

Three main Cretaceous arc sequences rest upon the CCOP (Reynaud et al., 1999; Kerr et al., 2002; Mamberti et al., 2003). In the coastal area it can be seen based on stratigraphic arguments that the Las Orquídeas and Cayo volcanic sequences of Coniacian–Campanian age conformably overlie the Piñon Formation that is part of the CCOP (Reynaud et al., 1999; Vanmelle et al., in press). In the northern part of the Cordillera Occidental, Boland et al. (2000) and Vallejo et al. (2006) identified the Río Cala island arc basement as being established on the CCOP.

The Macuchi island arc (Cosma et al., 1998; Chiaradia and Fontboté, 2001) is said to be mainly Eocene (Bourgeois et al., 1990), However, the FT age of 68 ± 11 Ma reported by Spikings et al. (2005) and the presence in some areas of radiolaritic red cherts as xenotliths in these rocks, similar to those found in the Late Cretaceous Cayo arc of the coastal area, suggests that the Macuchi terrane is also Late Cretaceous in age and was therefore initiated close to the Ecuadorian margin in a similar setting to the Río Cala or Cayo island arcs (Jaillard et al., in press). The Macuchi island arc would therefore also rest directly on the CCOP.

The location of the CCOPs eruption is largely debated, a common idea associates it to a hot-spot located close to the Galapagos hotspot's current location (Kerr and Tarney, 2005; Thompson et al., 2003). The CCOP would therefore have originated following the plume model described by Révillon et al. (1999, 2000) and Mamberti et al. (2003). This model explains the geochemical heterogeneities throughout the plateau marked by the existence of depleted picrites overlain by radiogenically (HIMU) and REE enriched ankaramites and Mg-basalts. The CCOP therefore carries a HIMU signature (Mamberti et al., 2003). However, other authors argue that the Galápagos hotspot was located too far from the Ecuadorian margin in Late Cretaceous times, to be responsible for the formation of the CCOP (Pindell et al., 2005; Jaillard et al., in press).

Four transverse sections through the Late Cretaceous island arcs are presented here (Fig. 1); all are purely intra-oceanic and show

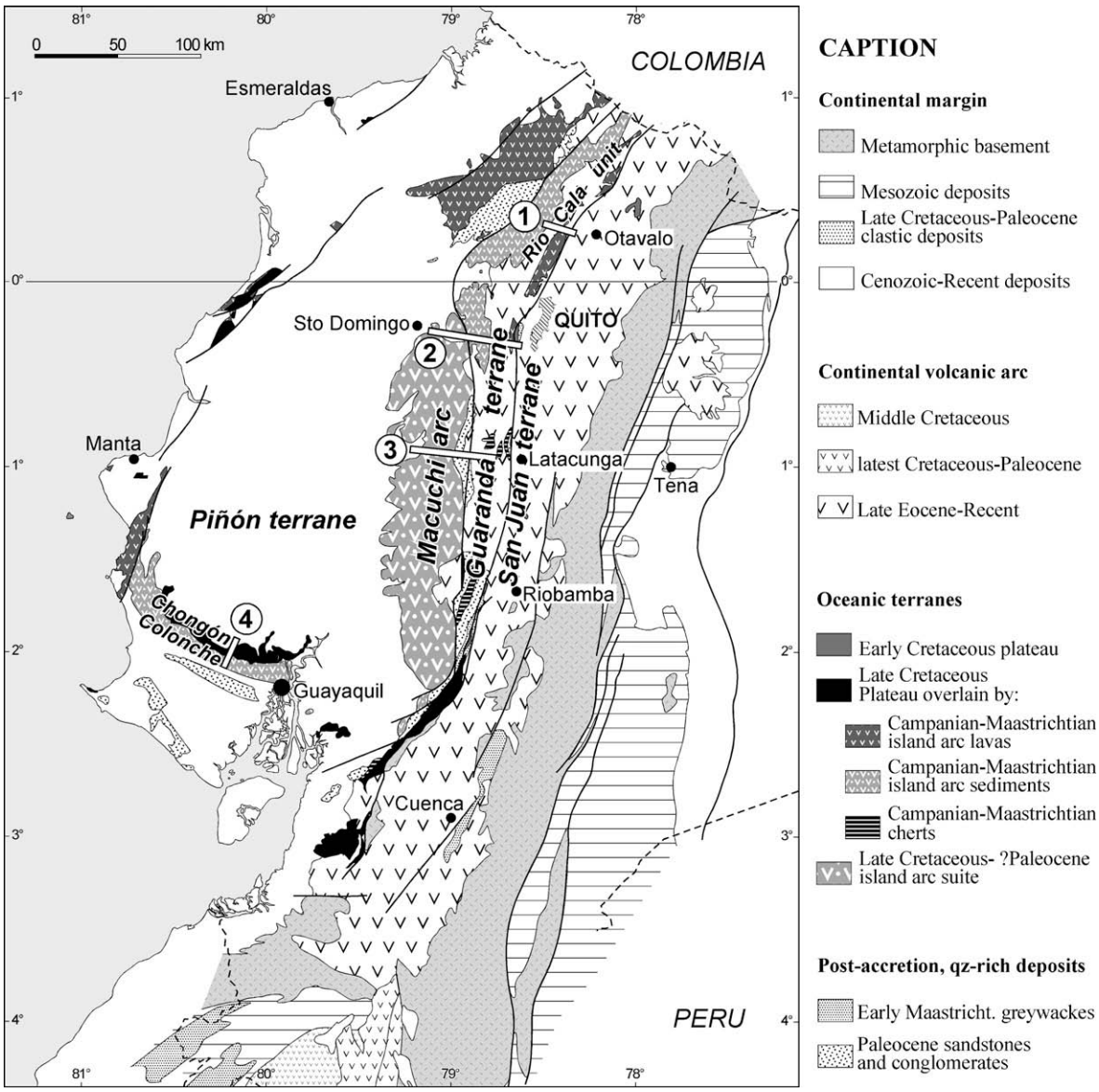

Fig. 1. Revised map of Ecuador showing main lithological units from cretaceous accretion episodes. Modified from Jaillard et al. (2004) and Jaillard et al. (in press). Numbers 1–4 are, respectively, Otavalo, Santo Domingo, Latacunga and La Derecha y Guaragua cross sections on which sampling was undertaken.

no evidence of continent-derived detritic sediments linked to their emplacement. The La Derecha and Guaragua sections exhibit the Las Orquídeas arc-like sequence and rest on the Piñon Formation close to Guayaquil (04.LD. and 04.GW. samples). The Latacunga (04.L. samples) and Santo Domingo sections (04.SD. samples) cuts through the Late Cretaceous to Paleogene Macuchi island-arc sequence in the Cordillera Occidental of Ecuador, close to Latacunga and Santo Domingo, respectively. Finally, the Otavalo section north of Quito crosscuts the Río Cala arc of Mid Campanian–Early Maastrichtian age (≈80–68 Ma, Boland et al., 2000).

In all four cases, the time lag between the formation of the CCOP and the island-arc emplacement is short (0–15 Ma, ≈2 Ma minimum according to Vallejo et al., 2006).

3. Analytical procedures

Wavelength-dispersive analyses for clinopyroxene major element compositions were made on a Cameca SX-50 electron microprobe fitted with five spectrometers at the Institute of Mineralogy and Geochemistry of the University of Lausanne. The standard procedures are 15 kV and 20 nA with an electron beam of 1 μm width and integrated counting times of 15 s on the background and 30 s on the peak. Synthetic and natural minerals were used as standards. A computer correction program (PAP) was used to calculate the effects of the crystal matrix on the element concentrations. The accuracy of major element determinations is better than ±1% of the total values.

Trace-element measurements on minerals were made by laser-ablation ICP-MS mass spectrometry using an Ar–F 193 nm Lambda Physics© Excimer laser coupled with a Perkin–Elmer 6100DRC ICP-MS at the Institute of Mineralogy and Geochemistry of the University of Lausanne. NIST610 and 612 glasses were used as external standards, Ca as internal standards after microprobe measurements on the pit sites. Ablation pit size varied from 40 to 80 μm depending on mineral size. BCR2 basaltic glass was regularly used as a monitor to check for reproducibility and accuracy of the system. Results were always within ±10% of the certified values.

Whole rock major- and trace-element concentrations were measured by a Philips PW 2400 XRF at the Centre d'Analyse Minérale, University of Lausanne. Complementary trace element concentrations were measured by ICP-MS VG-PQ2+ at the University Joseph Fourier of Grenoble following Barrat et al. (1996) procedures. Results for BHVO2 and BR2251 standards were always within ±4% of the certified values.

Isotope data were acquired on both whole-rocks and clinopyroxene separates. Samples were leached twice in a 2 N HCl 0.1 HF mixture and Nd separated according to analytical procedures described by Lapierre et al. (1997). Nd (dynamic acquisition) isotope ratios were measured at the Laboratoire de Géochimie isotopique, University Paul Sabatier (Toulouse) on a Finnigan MAT261 multicollector mass spectrometer. Results on standards yielded $^{143}Nd/^{144}Nd = 0.511850 \pm 0.000035$ (2σ external reproducibility) on 12 standard determinations. $^{143}Nd/^{144}Nd$ were normalized for mass fractionation relative to $^{146}Nd/^{144}Nd = 0.7219$, respectively. εNd_i was calculated with actual $(^{143}Nd/^{144}Nd)_{CHUR} = 0.512638$ and $(^{147}S/^{144}Nd)_{CHUR} = 0.1967$ (McCulloch and Wasserburg, 1978).

For lead separation, powdered samples were weighed to obtain approximately 200 ng of lead. Samples were leached with 6 N HCl during 30 min at 65 °C before acid digestion. They were dissolved for 48 h on a hotplate in a tri-distilled HF/HNO_3 mixture. After evaporation, 1 ml of HNO_3 was added to the residue and kept at about 90 °C for 12–24 h. After complete evaporation, 0.5 ml of 8 N HBr was added to the sample which was kept at 70 °C for 2–3 h before complete evaporation. The chemical separation of lead was done using 50 µl of anion exchange resin (AG1X8, 200–400 mesh) and samples were loaded and washed in 0.5 N HBr. Lead was then eluted in 6 N HCl. Pb blanks were less than 40 pg and are negligible for the present analyses.

Lead isotopes were analysed on a VG Plasma 54 multi-collector inductively coupled plasma-mass spectrometer (MC-ICP-MS) at the Ecole Normale Supérieure of Lyon. Lead isotope compositions were measured using the Tl normalization method described by White et al. (2000). For Pb isotope analysis, samples were bracketed between NIST 981 standards and calculated with respect to the standard value reported for this standard by Todt et al. (1996). This technique yields internal precision of ca. 50 ppm (2σ) and an external reproducibility of ca. 150 ppm (2σ) for 206Pb/204Pb ratios determined on 20 NIST standards.

All the isotopic data have been corrected for in situ decay using an age of 80 Ma.

4. Outcrop and sample description

The only complete cross-section that we present in this paper is the Otavalo cross-section, part of the Río Cala island-arc (Boland et al., 2000). The Otavalo cross-section crops out along the Otavalo-Selva Alegre road over 4.5–5 km and consists of a massive basaltic sequence formed by a pile-up of metric lava flows. The contact between each metric sequence is almost vertical, dipping steeply to the east. In each separate flow, a polarity is marked by an accumulation of pyroxene phenocrysts at the base and of plagioclase laths and vacuoles at the top of each flow. To the east, the flows are in fault-contact with Tertiary andesitic breccias, whilst to the west they are in fault-contact with Campanian–Maastrichtian greywackes which also dip steeply to the east (Mamberti, 2001).

For all the samples, from the four cross-sections the rock types have been distinguished on the basis of petrologic or textural attributes.

The basalts have very peculiar petrological attributes marked by the existence of centrimetric clinopyroxene phenocrysts that can, in Otavalo samples constitute up to 60–65% of the rock and measure up to 2 cm in length. Samples contain olivine with Cr-spinel inclusions, Cr-rich diopside and plagioclase in the matrix.

The most primitive basalt sample, 04 OT 01 contains olivine, altered to serpentine. This microlithic porphyric facies contains up to 60% pluri-centimetric clinopyroxene phenocrysts drowned in a microlithic matrix formed by plagioclase microliths. The crystallisation sequence in this rock type is olivine followed by clinopyroxene and oxide formation, whereas the crystallisation sequence in all other more differentiated samples is plagioclase followed by clinopyroxene, orthopyroxene and oxides.

Differentiated samples range from basalts – that contain both clinopyroxene and orthopyroxene, but no olivine, with rare plagioclase phenocrysts and a microlithic plagioclase matrix – to intersertal basalts characterised by the presence of 60% plagioclase laths that mark a form of fluidality around rare clinopyroxene phenocysts.

Finally, the most differentiated facies are andesites characterised by abundant plagioclase crystals surrounded by an aphyric vacuole-rich glass.

In all samples low degree burial-hydrothermal metamorphism is marked by the presence of smectite and pumpellyite and rare chlorite phases, igneous textures are always preserved.

5. Geochemical data

5.1. Whole rock geochemistry

5.1.1. Major element chemistry

The basalts, andesites have restricted SiO_2, TiO_2 (less than 1.1 wt.%, Table 1) and Al_2O_3 ranges (9–16 wt.%. Table 1). MgO values are typical of basaltic rocks (>5 wt.%) with the exception of sample 04 GW 01 (3.83 wt.%). Olivine bearing samples in the Otavalo and Latacunga cross sections show the highest MgO values (6–8 wt.%), whereas Santo Domingo, La Derecha and Guaragua samples have the low MgO values (3.83 wt.% minimum).

Classification of these lavas in the total alkali *vs.* silica diagram (Fig. 2a, TAS, Le Maıtre et al., 1989) reveals that the SiO_2 values for all the studied samples are within the basalt and basaltic-andesite fields. However, a large scatter of the total alkali values ($Na_2O + K_2O$ from 1.53 to 6.14 wt.%) reflects major element mobility caused by low degree burial-hydrothermal metamorphism and impedes on the classification.

The chemical classification based on Winchester and Floyd (1976) uses trace and major elements known as chemically stable during alteration and metamorphism. Fig. 2b is a binary diagram plotting TiO_2 against Y/Nb and shows that the studied samples have a tholeiitic affinity and plot in the Oceanic Tholeiitic Basalt (OTB) field. The high Y/Nb ratio reflects the LREE enrichment of the studied samples; this feature will be discussed in the following section.

5.1.2. Trace element chemistry

LILEs concentration variations reflect the high mobility of these elements during surface alteration and low degree burial metamorphism (Gibson et al., 1982). Sr, Pb, Th and U show very good linear correlations with Zr, indicating that these elements were little affected by such processes. Similarly, HFSE show no signs of mobility due to surface processes (Table 1).

The Otavalo lavas show the clearest correlations between trace elements and Zr, along with the highest compatible element concentrations. All but two mantle normalised multi-element spidergrams (Hofmann, 1988) show negative Nb, Ta anomalies (Fig. 3b). Such anomalies are typical of subduction-related magmatism. The presence of radiolaritic and doleritic inclusions in the two samples that do not show these anomalies mean that we cannot

Table 1
Major- (wt.%) and trace-element (ppm) analyses for Otavalo, Santo Domingo, Latacunga, La Derecha and Guaragua whole-rock samples ($Eu/Eu^* = Eu/((Sm + Gd)/2)$)

Sample	04OT1	04OT2	040T4a	040T4b	040T5	040T7	04SD01	04SD04	04SD05	04L04	04L05	04L10	04LD01	04GW-01
Name	Olivine basalt	Basalt	Basalt	Basalt	Basalt	Basalt	Andesite	Basalt	Basalt	Tuff	Basalt	Basalt	Dolerite	Dolerite
Locality	Otavalo	Otavalo	Otavalo	Otavalo	Otavalo	Otavalo	Santo Doming	Santo Doming	Santo Doming	Latacunga	Latacunga	Latacunga	La Derecha	Guaragua
SiO_2	56.08	50.94	49.61	49.81	48.07	51.24	54.76	48.51	51.70	50.65	50.07	50.45	50.69	53.70
TiO_2	0.61	0.81	1.05	0.81	0.78	0.76	0.99	0.73	0.76	0.62	0.44	0.71	0.54	1.14
Al_2O_3	14.86	16.52	14.29	14.64	16.49	15.00	15.64	15.55	16.69	17.83	9.70	14.45	15.95	15.23
Fe_2O_3	7.60	8.75	11.11	10.23	10.87	9.08	10.27	8.23	8.19	8.36	9.54	9.33	7.41	11.24
MnO	0.06	0.16	0.19	0.17	0.20	0.18	0.30	0.15	0.14	0.18	0.18	0.16	0.17	0.14
MgO	8.05	5.40	7.36	8.63	6.01	6.65	4.18	5.23	4.99	6.79	11.71	8.27	5.60	3.83
CaO	4.44	8.17	12.67	13.74	6.37	9.08	7.73	8.61	8.24	9.76	14.21	11.55	11.85	4.73
Na_2O	1.96	3.79	1.81	1.49	2.32	2.22	2.74	2.23	2.55	2.76	1.28	1.79	2.65	5.21
K_2O	1.73	2.26	0.10	0.04	3.53	2.45	1.01	2.91	2.77	0.46	0.47	1.96	0.37	0.93
P_2O_5	0.13	0.28	0.08	0.09	0.12	0.27	0.14	0.24	0.24	0.06	0.13	0.23	0.10	0.17
Loi	4.48	2.92	1.73	0.35	5.24	3.08	2.24	7.63	3.75	2.53	2.27	1.09	4.68	3.68
Sum	100	100	100	100	100	100	100	100	100	100	100	100	100	100
Cs	0.18	0.42	0.87	0.85	0.91	0.43	1.30	0.05	0.05	0.36	0.28	0.44	0.16	0.15
Rb	8.93	54.60	78.60	75.80	72.20	60.90	34.08	0.91	0.79	45.66	18.96	9.62	10.36	9.04
Ba	212	553	775	702	605	677	709.92	477.44	176.80	951.17	255.35	542.19	43.49	35.13
Th	0.63	2.31	3.13	3.29	2.97	3.14	0.75	0.23	0.16	1.32	2.21	1.37	0.64	0.61
U	0.23	0.79	1.04	1.10	0.97	1.03	0.19	0.08	0.05	0.43	0.73	0.84	0.19	0.20
Nb	0.84	3.12	3.49	3.69	3.91	3.89	0.97	4.09	2.73	1.05	3.42	1.91	1.16	1.05
Ta	0.05	0.13	0.15	0.16	0.18	0.17	0.06	0.34	0.17	0.07	0.19	0.11	0.07	0.06
Pb	1.02	1.37	3.30	3.33	3.07	3.32	2.22	0.73	0.36	3.46	7.65	3.71	1.42	1.40
Sr	305	756	1042	1123	777	808	148.67	105.07	97.77	237	403.71	388.65	293.41	315.17
Zr	26.10	78.80	99.90	105	108	104	42.74	43.20	29.95	47.88	110.43	118.80	42.23	38.08
Hf	0.72	1.92	2.44	2.55	2.59	2.50	1.08	1.32	0.85	1.46	2.79	3.13	1.20	1.05
Y	12.00	17.30	19.40	19.70	20.10	19.20	21.64	24.73	20.27	20.23	33.75	37.56	20.78	20.12
La	4.25	18.40	22.10	23.10	21.10	21.80	5.88	3.39	2.64	6.18	10.37	8.11	4.21	4.69
Ce	9.76	39.80	48.20	50.50	46.40	47.00	13.62	8.27	6.26	13.64	24.16	19.61	9.91	9.12
Pr	1.40	5.10	6.38	6.62	6.04	6.08	2.20	1.39	1.01	2.14	3.52	3.02	1.56	1.55
Nd	6.46	22.10	26.80	27.90	25.40	25.40	10.92	7.23	5.18	10.12	16.96	15.04	7.57	7.39
Sm	1.69	4.58	5.53	5.63	5.08	5.09	3.15	2.37	1.79	2.82	4.41	4.22	2.29	2.12
Eu	0.54	1.32	1.56	1.59	1.47	1.44	0.88	0.90	0.66	0.74	1.41	1.23	0.79	0.79
Gd	1.82	3.90	4.29	4.41	4.26	4.11	3.69	3.70	2.82	3.08	5.24	5.16	3.08	2.99
Tb	0.30	0.53	0.59	0.62	0.61	0.57	0.61	0.62	0.49	0.53	0.85	0.87	0.51	0.49
Dy	1.89	2.89	3.19	3.28	3.27	3.08	3.65	3.75	3.09	3.40	4.99	5.37	3.08	2.94
Ho	0.41	0.56	0.61	0.65	0.65	0.60	0.74	0.86	0.66	0.72	1.06	1.21	0.68	0.67
Er	1.21	1.49	1.68	1.77	1.83	1.67	2.06	2.47	1.88	2.20	3.12	3.51	2.04	1.90
Tm	–	–	–	–	–	–	–	–	–	–	–	–	–	–
Yb	1.12	1.36	1.53	1.59	1.66	1.55	1.96	2.99	2.21	2.50	3.81	4.26	2.42	2.44
Lu	0.17	0.21	0.24	0.25	0.26	0.24	0.29	0.41	0.32	0.36	0.53	0.64	0.35	0.35
(La/Yb)n	2.56	9.13	9.75	9.81	8.58	9.49	2.02	0.77	0.81	1.67	1.84	1.29	1.18	1.30
La/Nb_*	5.05	5.90	6.33	6.26	5.40	5.60	6.07	0.83	0.97	5.89	3.03	4.24	3.63	4.49
Eu/Eu^*	0.94	0.95	0.98	0.98	0.97	0.96	0.79	0.93	0.89	0.76	0.90	0.81	0.91	0.96

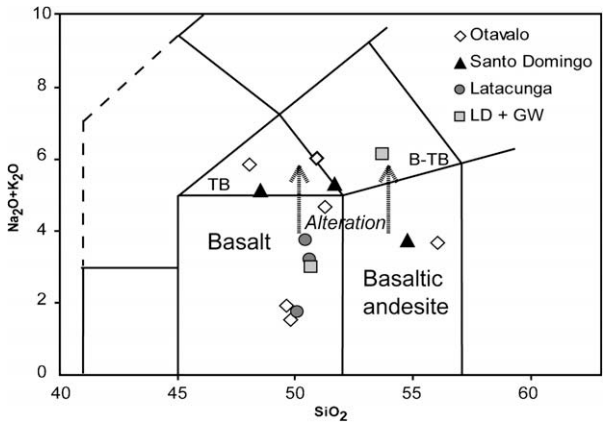

Fig. 2a. The Chemical classification and nomenclature of the Otavlo, Latacunga, Santo Domingo, La Derecha and Guaragua basalts and andesites using a total alkali (TAS) diagram (Le Maitre et al., 1989). B: Trachy-basalt, TB: Basaltic Trachyandesite.

consider their muti-element concentrations as representative of a magmatic process.

Otavalo rocks are geochemically very homogeneous and all have a positive Sr anomaly, this could reflect plagioclase accumulation in these samples. The olivine bearing 04 OT 01 basalt, has high MgO concentrations (8.05 wt.%) and also the lowest incompatible element concentrations (Fig. 3a). These characteristics could reflect its primitive nature. Chondrite normalised rare earth element plots (Hofmann, 1988) of Otavalo samples show LREE enriched trends ($(La/Yb)_n$ = 3.91–9.8). The Santo Domingo, Latacunga, La Derecha and Guaragua cross-sections contain more differentiated rocks (andesites) which explain their higher LREE contents.

Latacunga, Santo Domingo and La Derecha and Guaragua mantle-normalised multi-element spidergrams (Hofmann, 1988) are much less homogeneous in trace-element concentrations (Fig. 3b) than the Otavalo samples. Indeed, Santo Domingo lavas show a negative Pb anomaly and no Sr anomaly, whereas Latacunga lavas show positive Pb and Sr anomalies. The chondrite-normalised rare-earth element plots (Hofmann, 1988) for samples from these sections (Fig. 3a) show a slight LREE enrichment ($(La/Yb)_n$ = 1.3–1.8) and negative Eu anomalies (Eu/Eu^* = 0.79–0.9). Samples with the highest MgO concentrations systematically have the lowest LREE enrichment (04 OT 01, 04 OT 4a and 4b, 04 L 05). Once again, the two samples from the Santo Domingo section that have completely different REE and multi-element plots owe their chemical differences to the radiolaritic and doleritic inclusions they contain.

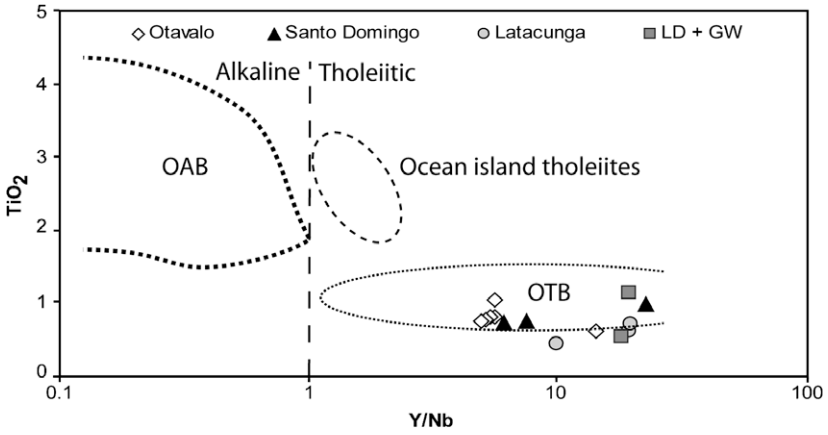

Fig. 2b. Distribution of TiO_2 and Y/Nb of the Otavlo, Latacunga, Santo Domingo, La Derecha and Guaragua basalts and andesites. OTB (oceanic tholeiitic basalt), OAB (oceanic alkaline basalt), ocean island tholeiites, alkaline and tholeiitic fields are from Winchester and Floyd (1976).

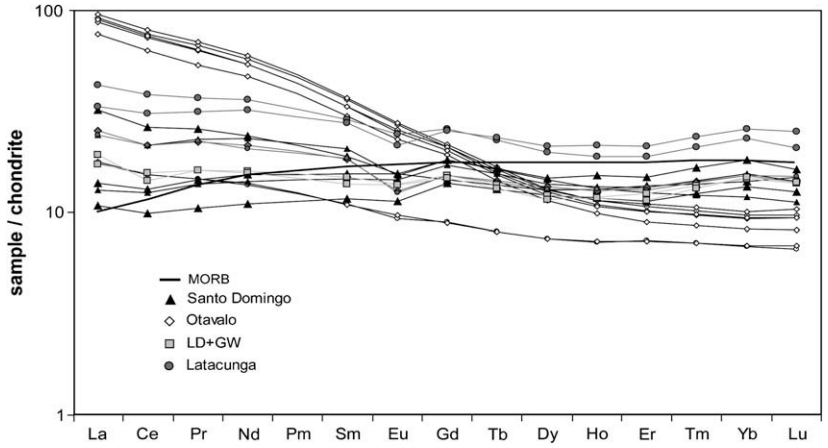

Fig. 3a. Chondrite-normalised REE patterns of all four sampled cross sections (Hofmann, 1988). Otavalo samples comprise Mamberti et al. (2003) Otavalo data. The MORB plot is from Saunders and Tarney (1984).

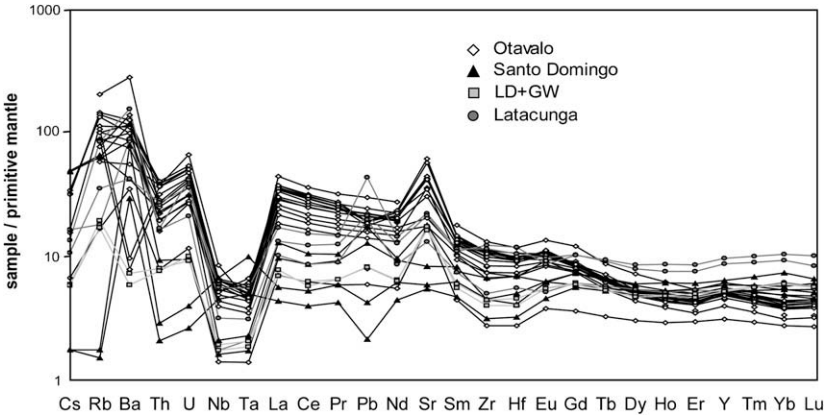

Fig. 3b. Primitive-mantle-normalised multi-element spidergrams of all four sample cross sections (Hofmann, 1988). Otavalo samples comprise Mamberti et al. (2003) Otavalo data.

6. Mineral chemistry

6.1. Major element chemistry

In this section, we choose to discuss clinopyroxene data from the Otavalo cross-section since Otavalo samples contain the largest and more abundant clinopyroxene phenocrysts. However, the chemical characteristics of clinopyroxenes from Latacunga, Santo Domingo, La Derecha and Guaragua are identical to those of Otavalo clinopyroxene phenocrysts.

Clinopyroxene phenocrysts are up to two centimetres in length but can also occur as 0.2 mm microphenocrysts in the matrix. Clinopyroxenes have a tholeiitic affinity, and belong to an island-arc context (Leterrier et al., 1982, Fig. 4a). The tholeiitic affinity of the clinopyroxene crystals is confirmed by chemical zoning within single clinopyroxene crystals.

Pyroxene cores have a diopsidic composition ($Wo_{45.2}$, $Fs_{5.8}$, Table 2) whereas the rims are augitic ($Wo_{36.8-41.1}$, $Fs_{12.4-21}$, Table 2) in the Morimoto et al. (1988), Fig. 4b classification diagram. This chemical variation within clinopyroxene phenocrysts can also be seen when opposing FeO, CaO, TiO_2 and Cr_2O_3 concentrations (Fig. 4c–f) to the XMg (=Mg/(Mg + Fe_t)). Crystal cores are FeO- and TiO_2-enriched in comparison to the CaO- and Cr_2O_3-enriched rims. This suggests that the growth of the clinopyroxene phenocrysts did not occur in melts of homogeneous composition, the cores were formed in Mg-rich melts whereas the rims crystallised from more differentiated magmas. Chemical variations within crystals are the same in large and small phenocrysts. This indicates that all clinopyroxene crystals belong to a single generation.

6.2. Trace element chemistry

Clinopyroxene trace-element compositions presented here belong only to the Otavalo 04 OT 01 sample, which has very large and fresh clinopyroxene phenocrysts. Clinopyroxene trace-element compositions in different samples show similar trends and concentrations as clinopyroxenes in Otavalo 04 OT 01 sample (Table 2) discussed below.

Mantle normalised multi-element spidergrams (Hofmann, 1988) show negative Nb, Ta, Pb and Zr anomalies (Fig. 5b). Crystal rims show higher trace-element compositions than the crystal cores. Additionally, crystal rims show a negative Eu anomaly that does not exist in crystal cores. This could mean that the end of clinopyroxene crystallisation is affected by plagioclase fractionation.

Chondrite-normalised REE plots (Hofmann, 1988) show that clinopyroxenes are LREE depleted (La/Yb = 0.27–0.8) and have a flat HREE plot (Fig. 5a). Crystal rims have higher REE concentrations than crystal cores. This could be explained by olivine fractionation that concentrates REE in the residual liquid from which the clinopyroxene crystals will form.

In order to test whether the clinopyroxene phenocrysts are in equilibrium with the host rock or whether they were inherited from an earlier crystallisation process, we attempted an approximate calculation of the clinopyroxene partition coefficients (Fig. 5c). In order to this, we made the assumption that samples are composed uniquely of 70% clinopyroxene crystals and calculated the partition coefficients for samples 04 OT 01. These calculated partition coefficients were then compared to partition coefficients documented by Fujimaki et al. (1984), Fig. 5c. We chose these particular partition coefficients in the literature as they were determined on natural pyroxenes rather than obtained experimentally for a given and narrow range of temperature and pressure. Fig. 5c illustrates that the calculated partition coefficients correlate well with those of Fujimaki et al., 1984. This confirms that the clinopyroxene phenocrysts are in equilibrium with the host-rock and were not inherited from an earlier crystallisation process.

7. Isotope data

The Sm, Nd and U, Th, Pb isotope systems are stable enough to be considered as unaffected by alteration processes. A slight Pb mobility when plotted against Zr can be noticed (not shown); however, a comparison of Pb isotope ratios to initial Pb isotope ratios shows that the age-correction has little effect on the presented lead isotope data (Table 3).

When plotting $(^{207}Pb/^{204}Pb)_i$ against $(^{206}Pb/^{204}Pb)_i$ (Fig. 6a), we can notice that all analysed samples plot in a restricted field above the NHRL (Zindler and Hart, 1986) defined by Chiaradia and Fontboté (2002), Fig. 6a – field 1 as the Ecuador Tertiary and Quaternary magmatism field. This field is 207Pb/204Pb enriched compared to the MORB field (Zindler and Hart, 1986) and spans out between the MORB and pelagic sediment fields (Sun, 1980; White et al., 1985; Ben Othman et al., 1994). Chiaradia and Fontboté (2001) suggested that the MORB field could be brought down to a more local component and compiled an East-Pacific MORB field (Sun, 1980; Cohen and O'Nions, 1982; Unruh and Tatsumoto, 1986). Analysed samples in this study span out between the East-Pacific MORB and enriched pelagic sediment fields.

We can note that whatever the XMg of samples, Pb isotope ratios are homogeneous suggesting that whatever the whole rock composition, samples reflect a unique source (Fig. 6b and c). Mamberti et al. (2003), Chiaradia and Fontboté (2001, 2002) and Chiaradia et al. (2004a,b) suggest the participation of a third high in U/Pb component (HIMU; Zindler and Hart, 1986).

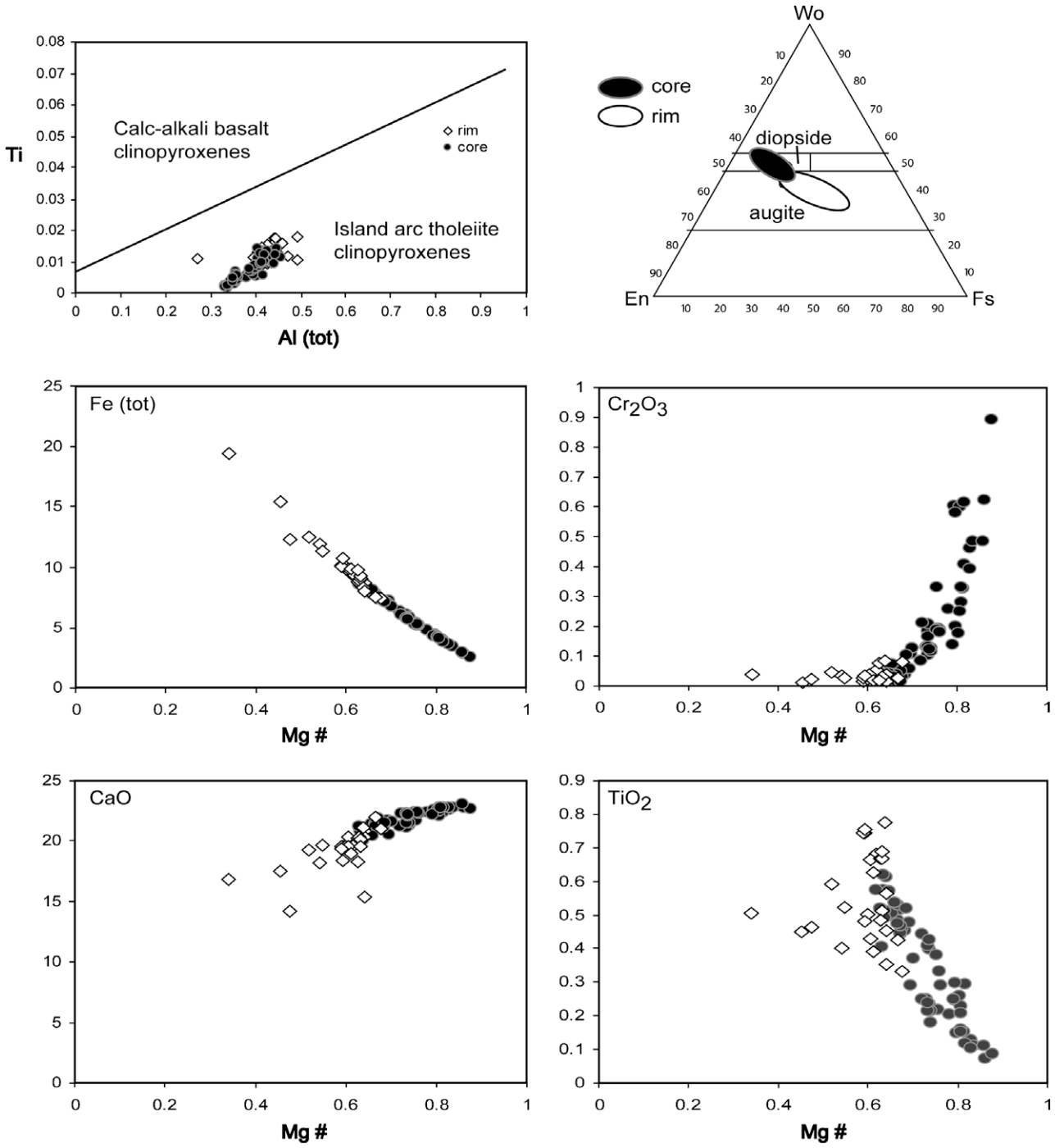

Fig. 4. (a) Clinopyroxene magmatic affinity (Ti *vs.* Ca + Na) (Leterrier et al., 1982) for Otavalo samples. (b) Clinopyroxene composition and classification diagram (Morimoto et al. (1988)) for Otavalo samples. (c)–(f). Clinopyroxene binary correlation diagrams, plotting major elements *vs.* XMg (XMg = Mg/(Mg + Fe)).

In order to explain the isotopic variations from one sample to the next we used a simple bipolar mixing model using an enriched pelagic sediment component and East-Pacific MORB end-members (not shown). However, this type of model was inappropriate since no mixing curve could be obtained to fit these variations.

Measured Nd and Pb isotope ratios can be explained by the mixing of three mantle end-members defined in literature as East-Pacific MORB (Chiaradia and Fontboté, 2001), HIMU (Zindler and Hart, 1986) and an enriched pelagic sediment component (Sun, 1980; White et al., 1985; Ben Othman et al., 1994; Mamberti et al., 2003). In order to test this hypothesis a tripolar mixing model according to the equations of Albarède, 1995 was used.

So as to fit to the regional geodynamic properties of such a natural system, the three mantle reservoirs have been modified using local geochemical data. The East-Pacific MORB or DMM reservoir value is the average of a data compilation according to McCulloch and Chappell (1982), Allègre et al. (1983), McCulloch and Black (1984), Peucat et al. (1988) and Goldstein et al. (1988) and East-Pacific MORB values from Chauvel and Blichert-Toft, 2001 and Hauff et al. (2003). The chert/pelagic sediment reservoir is a compilation of ratios for pelagic sediments found in latitudes from +2° to −2° dated as 70–100 Ma (Hauff et al., 2003). Finally, the value used for the HIMU component is the average value of the reservoir defined by Zindler and Hart (1986). The documented samples are

Table 2
Major- (wt.%) and trace-element (ppm) for Otavalo 04 OT 01, most representative clinopyroxene mineral samples

Name	Cpx1 rim	Cpx1 core	Cpx2 rim	Cpx2 core	Cpx2 rim	Cpx3 rim	Cpx3 rim	Cpx3 core	Cpx4 core	Cpx4 rim	Cpx5 rim	Cpx5 core	Cpx6 rim	Cpx6 core	Cpx7 core	Cpx8 core
SiO_2	50.12	53.46	51.38	52.99	51.55	50.73	51.55	53.36	51.73	49.89	49.32	53.75	50.63	51.73	51.53	51.00
TiO2	0.59	0.13	0.35	0.15	0.39	0.45	0.33	0.15	0.29	0.52	0.51	0.11	0.43	0.29	0.22	0.24
Al_2O_3	2.77	1.15	2.56	1.57	2.59	1.33	2.49	1.60	2.68	2.71	1.03	1.18	2.75	2.68	2.51	2.65
Cr_2O_3	0.05	0.46	0.04	0.20	0.02	0.01	0.08	0.33	0.11	0.03	0.04	0.48	0.03	0.11	0.33	0.18
FeO*	12.49	3.62	8.58	4.39	9.49	15.43	7.45	3.99	7.19	11.32	19.44	3.45	9.70	7.19	5.35	5.74
MnO	0.40	0.12	0.23	0.16	0.32	0.59	0.23	0.12	0.15	0.29	0.77	0.08	0.25	0.15	0.19	0.14
MgO	13.50	17.58	15.32	17.26	14.99	12.80	15.63	17.33	16.41	13.66	10.06	17.72	14.86	16.41	16.60	16.00
CaO	19.30	22.58	20.84	22.60	20.15	17.47	21.03	22.62	20.48	19.69	16.84	22.73	20.35	20.48	21.65	21.35
Na_2O	0.27	0.13	0.23	0.16	0.18	0.21	0.18	0.14	0.18	0.27	0.19	0.14	0.22	0.18	0.18	0.17
Sum	99.49	99.24	99.53	99.47	99.69	99.02	98.98	99.65	99.23	98.38	98.21	99.65	99.21	99.23	98.56	97.47
Si	1.90	1.96	1.92	1.95	1.93	1.95	1.93	1.95	1.92	1.91	1.95	1.96	1.91	1.92	1.92	1.92
Al IV	0.10	0.04	0.08	0.05	0.07	0.05	0.07	0.05	0.08	0.09	0.05	0.04	0.09	0.08	0.08	0.08
Al VI	0.03	0.01	0.03	0.02	0.04	0.01	0.04	0.02	0.04	0.03	0.00	0.01	0.03	0.04	0.03	0.04
Cr	0.00	0.01	0.00	0.01	0.00	0.00	0.00	0.01	0.00	0.00	0.00	0.01	0.00	0.00	0.01	0.01
Ti	0.02	0.00	0.01	0.00	0.01	0.01	0.01	0.00	0.01	0.02	0.02	0.00	0.01	0.01	0.01	0.01
Fe	0.40	0.11	0.27	0.13	0.30	0.50	0.23	0.12	0.22	0.36	0.64	0.11	0.31	0.22	0.17	0.18
Mn	0.01	0.00	0.01	0.01	0.01	0.02	0.01	0.00	0.00	0.01	0.03	0.00	0.01	0.00	0.01	0.00
Mg	0.76	0.96	0.85	0.95	0.83	0.73	0.87	0.95	0.91	0.78	0.59	0.97	0.83	0.91	0.92	0.90
Ca	0.79	0.89	0.83	0.89	0.81	0.72	0.84	0.89	0.82	0.81	0.72	0.89	0.82	0.82	0.86	0.86
Na	0.02	0.01	0.02	0.01	0.01	0.02	0.01	0.01	0.01	0.02	0.01	0.01	0.02	0.01	0.01	0.01
M1,2 sites	4.03	4.01	4.02	4.02	4.01	4.01	4.01	4.01	4.02	4.02	4.01	4.01	4.03	4.02	4.02	4.01
%En	38.9	49.0	43.4	47.9	42.8	37.4	44.5	48.3	46.5	39.7	30.2	49.2	42.3	46.5	47.1	46.1
%Fs	21.1	5.8	14.1	7.0	15.8	25.9	12.4	6.5	11.8	19.2	33.5	5.5	16.1	11.8	8.8	9.6
%Wo	40.0	45.2	42.4	45.1	41.4	36.7	43.1	45.3	41.7	41.1	36.3	45.3	41.6	41.7	44.1	44.2
Cs	0.00	0.00	0.01	0.01	0.02	0.00	0.02	0.01	0.01	0.02	0.00	0.00	0.00	0.00	0.00	0.02
Rb	0.01	0.00	0.02	0.02	0.29	0.02	0.01	0.01	0.07	0.16	0.07	0.08	0.00	0.00	0.00	0.02
Ba	0.49	0.22	0.00	0.14	3.01	0.01	0.47	0.00	0.51	2.09	1.36	0.46	0.03	0.04	0.04	0.16
Th	0.00	0.01	0.01	0.00	0.01	-	0.01	0.00	0.01	0.06	0.03	0.01	0.00	0.00	0.00	0.00
U	0.01	0.00	0.00	0.00	0.01	-	0.01	0.00	0.00	0.01	0.00	0.00	0.00	0.00	0.00	0.01
Nb	0.00	0.01	0.01	0.01	0.03	0.00	0.00	0.00	0.01	0.01	0.08	0.01	0.00	0.00	0.00	0.02
Ta	0.00	-	0.00	0.00	0.00	0.00	0.00	0.00	-	0.00	0.00	0.00	0.00	0.00	0.00	0.00
Pb	0.24	0.50	0.28	0.22	0.26	0.02	0.36	0.06	0.09	1.59	0.63	0.42	0.09	0.10	0.10	0.39
Sr	2.38	2.25	2.52	2.19	2.86	2.05	2.58	2.00	2.06	2.49	2.30	2.44	2.21	2.36	2.34	2.67
Zr	0.11	0.02	0.14	0.08	0.11	0.02	0.10	0.01	0.01	0.21	0.05	0.05	0.02	0.02	0.02	0.04
Hf	0.13	0.02	0.24	0.12	0.14	0.02	0.16	0.01	0.02	0.38	0.06	0.07	0.05	0.05	0.05	0.04
Y	2.48	0.65	2.79	1.91	2.09	0.62	2.18	0.34	0.40	3.85	1.24	1.39	0.77	0.82	0.81	1.19
La	14.12	4.00	13.23	8.93	13.85	3.97	17.77	1.36	3.59	28.18	14.77	8.99	4.48	4.78	4.75	7.86
Ce	0.40	0.13	0.41	0.32	0.38	0.11	0.43	0.05	0.07	0.58	0.34	0.21	0.12	0.13	0.13	0.22
Pr	15.58	4.34	16.06	11.73	13.73	3.81	15.82	2.09	2.81	18.79	10.52	7.15	4.82	5.14	5.10	8.47
Nd	0.54	0.14	0.61	0.46	0.51	0.16	0.54	0.09	0.11	0.72	0.36	0.29	0.18	0.19	0.19	0.31
Sm	0.38	0.10	0.40	0.30	0.35	0.09	0.37	0.04	0.07	0.52	0.17	0.19	0.13	0.14	0.14	0.18
Eu	1.26	0.30	1.22	0.89	1.15	0.27	1.15	0.24	0.19	1.54	0.48	0.54	0.37	0.40	0.39	0.63
Gd	–	–	–	–	–	–	–	–	–	–	–	–	–	–	–	–
Tb	1.52	0.46	1.71	1.19	1.13	0.48	1.26	0.22	0.23	2.16	0.71	0.81	0.50	0.53	0.52	0.69
Dy	0.38	0.08	0.38	0.27	0.31	0.07	0.29	0.06	0.05	0.51	0.18	0.19	0.10	0.11	0.11	0.19
Ho	1.17	0.23	1.09	0.76	0.82	0.25	0.84	0.13	0.18	1.52	0.44	0.61	0.28	0.29	0.29	0.45
Er	9.86	1.90	10.70	7.35	7.95	1.83	7.63	1.27	1.58	12.80	4.84	4.63	2.67	2.84	2.82	4.43
Tm	–	–	–	–	–	–	–	–	–	–	–	–	–	–	–	–
Yb	0.84	0.20	0.78	0.64	0.74	0.10	0.70	0.05	0.11	1.27	0.43	0.45	0.39	0.42	0.41	0.06
Lu	0.12	0.04	0.15	0.11	0.11	0.02	0.10	0.01	0.02	0.20	0.07	0.07	0.06	0.06	0.06	0.43

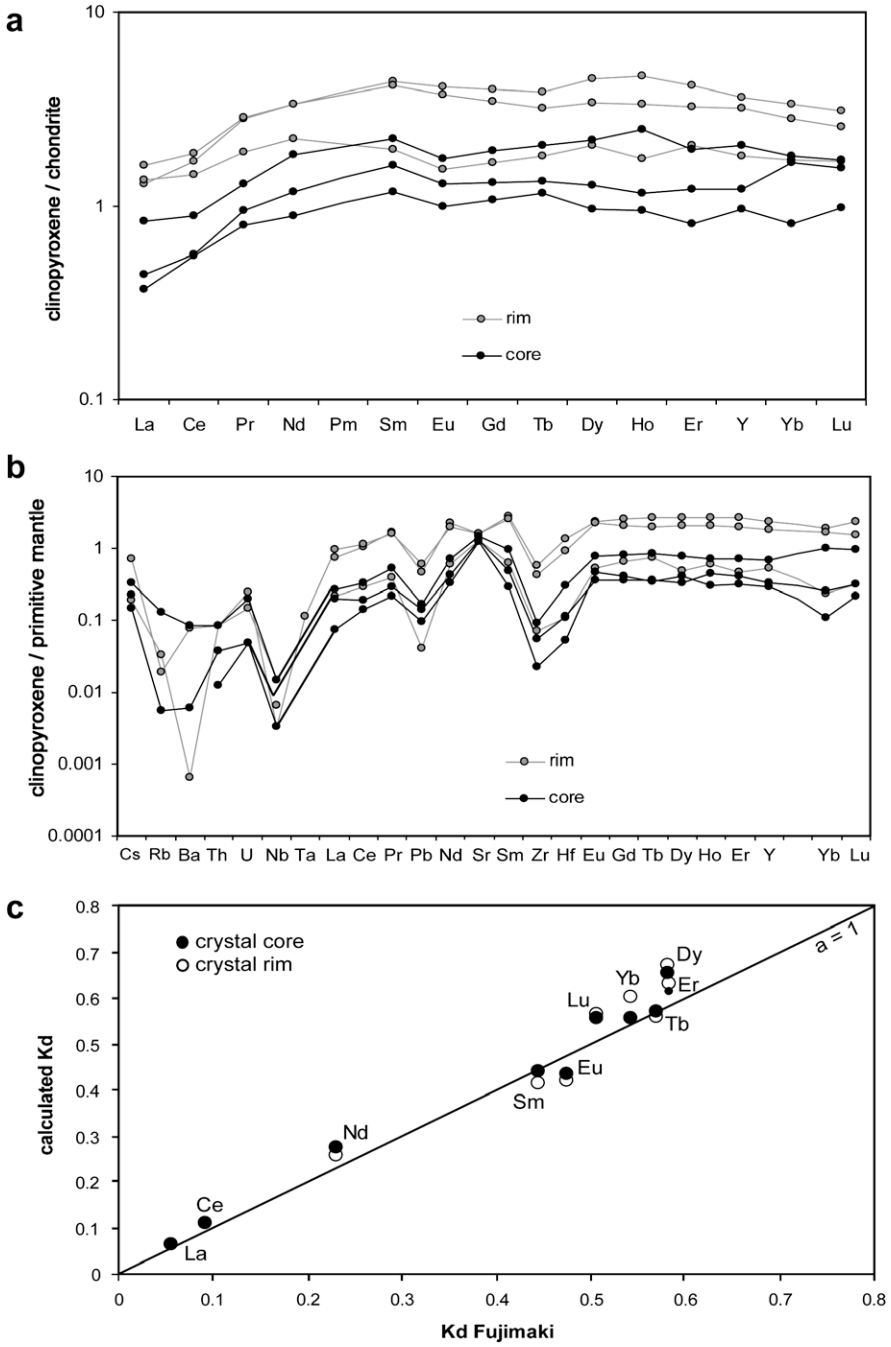

Fig. 5. (a) Chondrite-normalised REE patterns, and (b) Primitive-mantle-normalised multi-element spidergrams (Hofmann, 1988), for 04 OT 01 clinopyroxenes. (c) Binary correlation diagram of calculated clinopyroxene REE partition coefficients and clinopyroxene REE partition coefficients from Fujimaki et al. (1984).

not precisely of the same age and latitude as CCOP at the time of the Cretaceous arc emplacement, we therefore chose to compile a large amount of data and use the average values of this compilation.

The Figs. 7a and b respectively show plots of $(^{143}Nd/^{144}Nd)_i$ *vs.* $(^{206}Pb/^{204}Pb)_i$ and $(^{207}Pb/^{204}Pb)_i$. We can notice that in both cases samples plot in a very narrow field that can be explained by the mixing of variable proportions of the three end-members.

Indeed, 12–15% of the HIMU component has to be mixed to the DMM end member so as to explain sample chemistry. Additionally, variable proportions (7–15%) of the chert/pelagic sediment end-member are also needed to explain whole rock isotope ratios. Such high HIMU components are rarely obtained in tripolar mixing models and could partly be linked to the lack of constraint on mantle end-members such as the HIMU reservoir. However, as we discuss in the following section, such high percentages could also be linked to the uncommon geodynamic context from which these magmas are derived.

8. Discussion and geodynamic implications

Four cross-sections through three late-Cretaceous to early Paleocene island arc sequences directly overlying the CCOP are studied in this paper. Samples are mainly basalts and andesites that are marked by the existence of centrimetric clinopyroxene phenocrysts that can, in Otavalo samples, constitute up to 60–

Table 3
Nd and Pb isotopic compositions for Otavalo, Santo Domingo, Latacunga, La Derecha and Guaragua whole-rock samples and mineral separates

Name	T(My)	Sm	Nd	206Pb/204Pb	±2σ	207Pb/204Pb	±2σ	208Pb/204Pb	±2σ	(206Pb/204Pb)$_i$	(207Pb/204Pb)$_i$	(208Pb/204Pb)$_i$	143Nd/144Nd	±2σ	147Sm/144Nd	(143Nd/144Nd)$_i$	Eps(Nd)$_i$
04 OT 1	80	1.69	6.46	18.7838	*0.0042*	15.6046	*0.0052*	38.6178	*0.0063*	18.2823	15.5906	38.1965	0.512900	*0.000007*	0.158169	0.512817	5.51
04 OT 2	80	4.58	22.10	19.0174	*0.0039*	15.4503	*0.0042*	38.3997	*0.0052*	18.5644	15.4285	37.9618	0.512834	*0.000008*	0.125295	0.512768	4.55
04 OT 4a	80	5.53	26.80	18.9102	*0.0037*	15.5868	*0.0046*	38.6715	*0.0054*	18.6613	15.5749	38.4242	0.512828	*0.000010*	0.124753	0.512763	4.44
04 SD 01	80	3.15	10.92	18.9940	*0.0026*	15.6478	*0.0042*	38.7744	*0.0050*	18.7899	15.6380	37.9930	0.512981	*0.000008*	0.174504	0.512890	6.92
04 SD 04	80	2.37	7.23	18.9599	*0.0086*	15.5665	*0.0089*	38.6109	*0.0102*	18.6863	15.5533	37.7820	0.513007	*0.000012*	0.198615	0.512903	7.18
04 SD 05	80	1.79	5.18	19.0012	*0.0090*	15.5758	*0.0091*	38.6857	*0.0140*	18.7518	15.5638	38.1099	0.513039	*0.000009*	0.208795	0.512930	7.70
04 L 04	80	2.82	10.12	–	–	–	–	–	–	–	–	–	0.512899	*0.000009*	0.168572	0.512811	5.38
04 L 05	80	4.41	16.96	18.6878	*0.0076*	15.5193	*0.0086*	37.2554	*0.0071*	16.4393	15.5073	36.3995	0.512949	*0.000006*	0.157324	0.512867	6.47
04 LD 01	80	2.29	7.57	18.8692	*0.0046*	15.6036	*0.0051*	38.5274	*0.0068*	18.6424	15.5927	37.9523	0.513014	*0.000015*	0.182643	0.512918	7.48
04 GW 01	80	2.12	7.39	18.8886	*0.0050*	15.6002	*0.0056*	38.5161	*0.0063*	18.6298	15.5877	37.9217	0.512975	*0.000008*	0.173503	0.512884	6.81
04OT1cpx	80	0.71	1.73	–	–	–	–	–	–	–	–	–	0.512941	*0.000011*	0.246862	0.512812	5.40
04OT4acpx	80	1.49	4.46	–	–	–	–	–	–	–	–	–	0.512736	*0.000008*	0.202338	0.512630	1.85
04OT4bcpx	80	2.91	9.26	18.7852	*0.015*	15.6338	*0.0157*	38.6320	*0.0144*	18.7639	15.6328	38.5546	0.512879	*0.000007*	0.190131	0.512779	4.77
04Ot5cpx	80	4.13	12.32	19.0024	*0.0317*	15.7067	*0.0329*	38.9703	*0.0341*	18.9738	15.7054	38.9366	0.512885	*0.000008*	0.202824	0.512779	4.76
04OT7cpx	80	3.69	11.72	18.8903	*0.0049*	15.5900	*0.0069*	38.6166	*0.0077*	18.8391	15.5875	38.5627	0.512852	*0.000012*	0.190237	0.512752	4.24

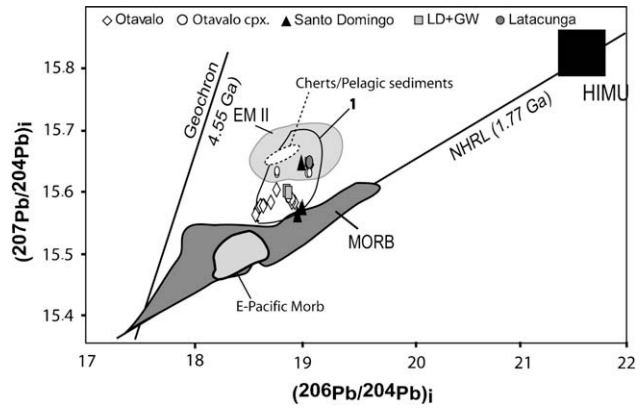

Fig. 6a. $(^{207}Pb/^{204}Pb)_i$ *vs.* $(^{206}Pb/^{204}Pb)_i$ of all four cross sections together with the compositional fields of the main mantle reservoirs of Zindler and Hart (1986). Also shown are the fields of East-pacific MORB (Unruh and Tatsumoto, 1986; Cohen and O'Nions, 1982; Sun, 1980), and the North Hemisphere Reference Line (NHRL) of Hart (1984). Field 1 represents Ecuador tertiary magmatism isotopic ratios (Chiaradia and Fontboté, 2001). Otavalo samples comprise Mamberti et al. (2003) Otavalo data.

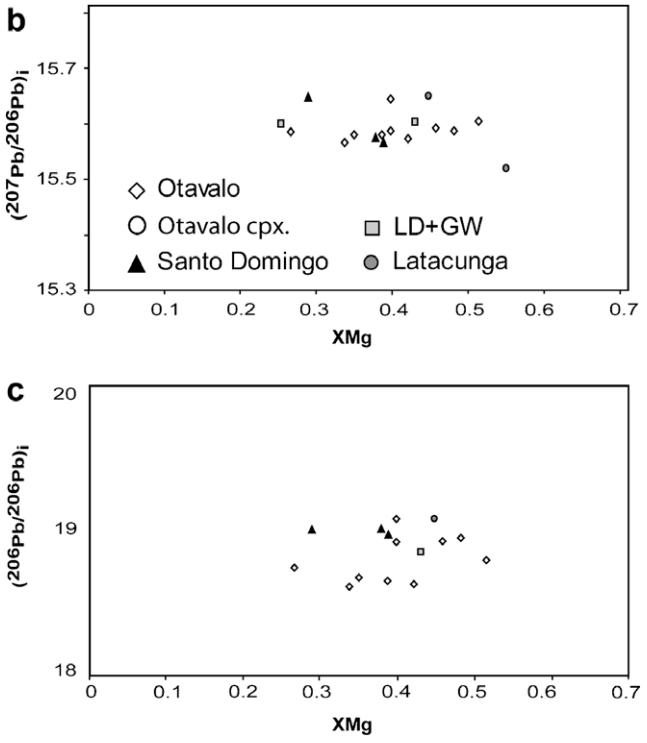

Fig. 6b and c. Plot of $(^{207}Pb/^{204}Pb)_i$ and (c) $(^{206}Pb/^{204}Pb)_i$ *vs.* XMg. (XMg = Mg/(Mg + Fe)). Otavalo samples comprise Mamberti et al. (2003) Otavalo data.

65% of the rock and measure up to 2 cm in length but can also occur as 0.2 mm microphenocrysts in the matrix. Clinopyroxenes are chemically zoned (Fig. 4b–f) with diopsidic ($Wo_{45.2}$, $Fs_{5.8}$, Table 2) cores and augitic rims ($Wo_{36.8–41.1}$, $Fs_{12.4–21}$, Table 2) and are in equilibrium with the host lava (Fig. 5c). This petrological particularity is not uncommon in island arc rocks but strongly resembles descriptions of arc picrites in the Solomon islands by Ramsay et al. (1984) and the ankaramitic facies and Mg-basalts that constitute parts of the CCOP (Mamberti et al., 2003).

Basalt and andesite samples of the Otavalo cross-section through the Rio Cala island arc (Boland et al., 2000), the Latacunga and Santo Domingo cross-sections through the Macuchi arc (Jail-

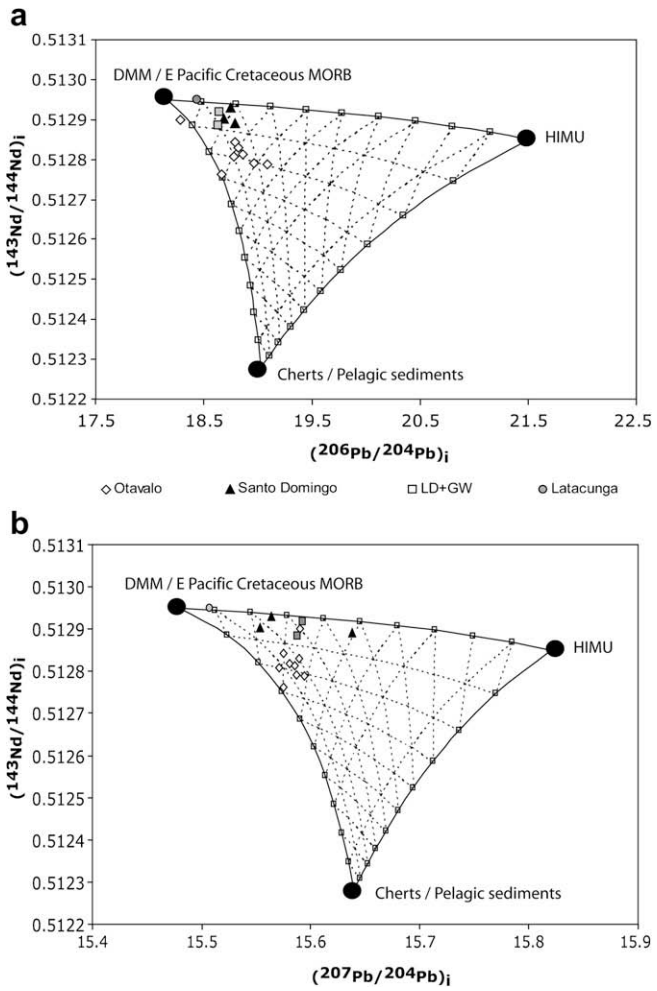

Fig. 7. (a) Tripolar mixing modelisation diagram plotting $(^{143}Nd/^{144}Nd)_i$ *vs.* $(^{206}Pb/^{204}Pb)_i$ and (b) $(^{143}Nd/^{144}Nd)_i$ *vs.* $(^{207}Pb/^{204}Pb)_i$. The HIMU mantle reservoir shown here is the barycentre of Zindler and Hart (1986) HIMU field. The cherts/Pelagic sediment reservoir are an average composition for cherts dated from 70 to 100 Ma by Hauff et al. (2003). The DMM/Pacific Cretaceous MORB is an average of DMM ratios by McCulloch and Chappell (1982), Allègre et al. (1983), McCulloch and Black (1984), Peucat et al. (1988) and Goldstein et al. (1988), and E-pacific Morb values from Chauvel and Blichert-Toft (2001) and Hauff et al. (2003).

lard et al., 2004; Spikings et al., 2005) and the La Derecha and Guaragua cross-sections through the Las Orquìdeas arc-like sequence (Luzieux et al., 2006) are Mg-rich (6–11.5 wt.%) are LREE enriched ($(La/Yb)_n$ = 3.91–9.8). The high proportions of clinopyroxene and the high MgO contents of these rocks indicate a high percentage of partial melting at the magmatic source. The origin of the LREE enrichment of the Mg-rich basalts can be found in the involvement of subducted pelagic sediments in the genesis of these lavas as suggested by Mamberti et al. (2003) in their study of Ecuador.

The four sampled cross-sections through the island-arc sequences display homogeneous initial Nd, and Pb isotope ratios that suggest a unique mantellic source for these rocks. This is confirmed by the homogeneity of lead isotope ratios with varying XMg of the different lavas (Fig. 6b and c). Plots of $(^{207}Pb/^{204}Pb)_i$ *vs.* $(^{206}Pb/^{204}Pb)_i$ (Fig. 6a) show that the analysed samples plot in a restricted field within the Ecuador Tertiary and Quaternary magmatism field defined by Chiaradia and Fontboté (2002) Fig. 6a – field 1. This field spans out between the E-pacific MORB (Sun, 1980; Cohen and O'Nions, 1982; Unruh and Tatsumoto, 1986; Chiaradia and Fontboté, 2002) and pelagic sediment fields (Sun, 1980; White et al., 1985; Ben Othman et al., 1994; Mamberti et al., 2003). Measured Pb and Nd isotopic ratios suggest the participation of a third HIMU component. The Pb and Nd isotope ratios can thus be explained the mixing of three components: an East-Pacific MORB end-member, an enriched pelagic sediment component, and a HIMU component as suggested by previous authors such as Chiaradia and Fontboté (2001), Mamberti et al. (2003) and Vallejo et al. (2006).

Mamberti et al. (2003) showed that the ankaramite and Mg-basalts that constitute the CCOP carry a HIMU component. The isotopic, geochemical and petrological properties of the studied lavas could therefore mark the contribution of the CCOP in the genesis of these island arc rocks.

This study suggests that by better constraining the three end-members and by attempting to fit to the regional natural system in which these lavas were generated, it is possible to estimate the influence of each end-member on sample isotopic ratios. Indeed, the DMM/East Pacific MORB component can be brought down to a local value obtained by compiling published DMM and East-Pacific MORB values from McCulloch and Chappell (1982), Allègre et al. (1983), McCulloch and Black (1984), Peucat et al. (1988), Goldstein et al. (1988), Chauvel and Blichert-Toft (2001) and Hauff et al. (2003). The pelagic radiolarian bearing sediments are represented by the Campano-Maastrichtien cherts found associtiated with the late Cretaceous island arc volcanics and are taken from compilation of isotopic ratios for pelagic sediments found in latitudes from +2° to −2° dated as 70–100 Ma from Hauff et al. (2003). Finally, the HIMU (Zindler and Hart, 1986) end-member represents the radiogenically enriched CCOP upon which the island arcs rest.

Mathematically, an average contribution of 12–15 wt.% HIMU/CCOP associated with 7–15 wt.% cherts and to 70–75 wt.% DMM is needed to explain sample isotopic ratios (Fig. 7).

Chiaradia and Fontboté (2001, 2002) had already suggested that 10 wt.% subducted sediments were needed to explain sample chemistry; however this is surprisingly high when compared to the 2–3 wt.% sediment dehydration usually observed in subduction systems. Similarly, it may seem that 12–15 wt.% plateau contribution is also high.

We suggest that an anomalous thermal regime could be responsible for such high proportions of the HIMU/CCOP component during lava genesis. Such a high thermal regime could be inherited from the young and residually hot CCOP. Indeed, the studied arc-like and island arc sequences established themselves in Campanian-Maastrichtian (75–80 Ma) to early Palaeocene (68 Ma) times on a young (Vallejo et al., 2006) and therefore probably still hot oceanic plateau emplaced at 92–86 Ma (Sinton et al., 1998; Mamberti et al., 2003). The buoyant and thick CCOP would therefore be 5–15 Ma-old at the time of arc emplacement, and would not have dissipated the heat inherited from its formation at the plateau base.

Four main mechanisms could be responsible for the isotopic mixing described in this study. Firstly Chiaradia and Fontboté (2001, 2002) and Chiaradia et al. (2004a,b) identified a HIMU component in Ecuadorian Late Cretaceous and Tertiary magmas and ascribed it to two possible processes: diffusion of the 90 My old Galapagos or the 106–82 My old Oriente hot-spot into the upper mantle or the subduction and recycling by mantle and crustal processes of oceanic plateaus created during the mid-Cretaceous superplume event. However, we believe that this process could not generate the high proportions of HIMU component needed to explain the isotopic compositions of the studied arc rocks. A second hypothesis could be that when the island arc established itself on the CCOP, magma pooled in a magma chamber within the CCOP and assimilated the chamber wall rock, this would mean that the radiogenic signature of the lavas is linked to the amount of time spent in the magma chamber, the more primitive magma would therefore be less affected by the assimilation process than the

more differentiated samples. Yet Fig. 6b and c shows that the radiogenic signature of these arc rocks is independent from the MgO content of samples and therefore do not depend on the degree of differentiation undergone by the magmas. Finally, considering the high temperature beneath the CCOP at that time, it is possible that melting of plateau base could be responsible for these radiogenic isotope ratios. Indeed, the amount of dehydration of the subducted cherts could destabilise the upper mantle into which is subducted, generating mantle-derived basaltic melts that could accumulate at the base of the still hot CCOP and partially melt and assimilate it. This process could explain the large contribution of the HIMU and EM2-type end members during the genesis of the studied island arc lavas.

However, the poor constraint of the HIMU-plateau isotope ratios in the case of the CCOP due to plateau heterogeneity (Révillon et al., 1999; Mamberti et al., 2003) could have exaggerated the contribution of the HIMU end-member, making it impossible to rule out the first hypothesis made by Chiaradia and Fontboté (2001, 2002).

9. Conclusions

The mineralogical and geochemical particularities of Late Cretaceous arc-like or island-arc sequences established on the Caribbean–Colombian Oceanic Plateau suggest the existence of an abnormally high heat regime during magma genesis, much like in the Plio-Quaternary arc of the Solomon islands caused by the subduction of the young and hot Woodlark basin below the Cretaceous Ontong Java oceanic plateau that accreted to the Vityaz arc 10 Ma ago.

This geochemical study of samples from four Late Cretaceous arc-like or island arc sequences points to the participation of three mantle reservoirs at the magma source. This is confirmed by the whole rock isotope ratio trends obtained for all four sampled sections.

A tripolar mixing model reveals itself to be appropriate and suggests that proportions of 12–15 wt.% of the HIMU component and 7–15 wt.% of the pelagic sediment end-member and 70–75 wt.% DMM-East-Pacific MORB are needed to explain sample isotope ratios. These surprisingly high proportions of the HIMU component (carried by the oceanic plateau) can be explained by the young age of the CCOP (5–10 Ma) when the Late Cretaceous volcanic sequences developed. Indeed, the young CCOP would have carried an important amount of residual heat at the time of arc emplacement.

The hot CCOP basement of these arc sequences was probably easily assimilated at the island arc lava source. This could reflect a process such as plateau base melting resulting from release of fluids into the upper mantle following the high dehydration degree of subducted pelagic sediments.

Acknowledgement

This study was initiated by Henriette Lapierre. A very passionate and devoted colleague, she played an important role in this project as in many others. She was a friend for all of us. The field trip was financially supported by the Institut de Recherche pour le Développement (IRD, France), and indirectly by OXY-Ecuador. This study is part of a Dyeti project (France). This manuscript was improved by the thorough reviews of Massimo Chiaradia and an anonymous reviewer.

References

Albarède, F., 1995. Introduction to Geochemical Modeling. Cambridge University Press. pp. 1–52.

Allègre, C.J., Hart, S.R., Minster, J.F., 1983. Chemical structure and evolution of the mantle and continents determined by inversion of Nd and Sr idotopic data, II. Numerical experiments and discussion. Earth and Planetary Science Letters 66, 191–213.

Barrat, J.A., Keller, F., Amosse, J., Taylor, R.N., Nesbitt, R.W., Hirata, T., 1996. Determination of the rare earth elements in sixteen reference samples by ICP-MS after Tm addition and ion exchange separation. Geostandards Newsletter 20, 133–139.

Ben Othman, D., White, W.M., Patchett, J., 1994. The geochemistry of marine sediments, island arc, magma genesis, and crust-mantle recycling. Earth and Planetary Science Letters 94, 1–21.

Boland, M.P., McCourt, W.J., Beate B., 2000. Mapa geológico de la Cordillera Occidental del Ecuador entre 0°–1°N, escala 1/200,000. Minist. Energ. Min.-BGS publs., Quito.

Bourgeois, J., Egüez, A., Butterlin, J., De Wever, P., 1990. Evolution géodynamique de la Cordillère Occidentale des Andes d'Equateur: La découverte de la formation océanique d'Apagua. C.R. Académie des Sciences Paris (II) 311, 173–180.

Chauvel, C., Blichert-Toft, J., 2001. A Hafnium isotope and trace element perspective on melting of the depleted mantle. Earth and Planetary Science Letters 190, 131–151.

Chiaradia, M., Fontboté, L., 2001. Radiogenic lead signatures in Au-rich volcanic-hosted massive sufide ores and associated volcanic rocks of the early Tertiary Macuchi island arc (Western Cordillera of Ecuador). Economic Geology 96, 1361–1378.

Chiaradia, M., Fontboté, L., 2002. Lead isotope systematics of Late Cretaceous – Tertiary Andean arc magmas and associated ores between 8°N and 40°S: evidence for latitudinal mantle heterogeneity beneath the Andes. Terra Nova 14, 337–342.

Chiaradia, M., Fontboté, L., Beate, B., 2004a. Cenozoic continental arc magmatism and associated mineralization in Ecuador. Mineralium Deposita 39, 204–222.

Chiaradia, M., Fontboté, L., Paladines, A., 2004b. Metal sources in mineral deposits and crustal rocks of Ecuador (1°N–4°S): a Lead isotope synthesis. Economic Geology 99, 1085–1106.

Cohen, R.S., O'Nions, R.K., 1982. The lead, neodymium and strontium isotopic structure of Ocean ridge basalts. Journal of Petrology 23, 299–324.

Cosma, L., Lapierre, H., Jaillard, E., Laubacher, G., Bosch, D., Desmet, A., Mamberti, M., Gabrielle, P., 1998. Pétrographie et géochimie des unités magmatiques de la cordillère occidentale d'Equateur (0°30′S): implications tectoniques. Bulletin de la Société Géologique de France 6, 739–751.

Feininger, T., Bristow, C.R., 1980. Cretaceous and Palaeogene history of coastal Ecuador. Geologische Rundeschau 69, 849–874.

Fujimaki, H., Tatsumoto, M., Aoki, K., 1984. Partition coefficients of Hf, Zr and REE between phenocrysts and groundmasses. Proceedings of the fourteenth lunar and planetary science conference, Part 2. Journal of Geophysical Research 89 (suppl.), B662–B672.

Gardien, V., Lécuyer, F., Moyen, J.F., 2008. Dolerites of the Woodlark Basin (Papuan Peninsula, New Guinea): a geochemical record of the influence of a neighbouring subduction zone. Journal of Asian Earth Sciences 33 (3–4), 139–154.

Gibson, S.A., Kirkpatrick, R.J., Emmermann, R., Schmincke, P.H., Pritchard, G., Okay, P.J., Thorpe, R.S., Marriner, G.F., 1982. The trace element composition of lavas and dykes from a 3 km vertical section through a lava pile in eastern Island. Journal of Geophysical Research 87, 6532–6546.

Goldstein, S.L., O'Nions, R.K., Hamilton, P.J., 1988. Decoupled evolution of Nd and Sr isotopes in the continental crust. Nature 336, 733–738.

Hart, S.R., 1984. A large-scale isotope anomaly in Southern Hemisphere mantle. Nature 309, 753–757.

Hauff, F., Hoernle, G., Tilton, G., Graham, W., Kerr, A.C., 2000. Large volume recycling of oceanic lithosphere over short time scales: geological constraints from the Caribbean Large Igneous Province. Earth and Planetary Science Letters 174, 247–263.

Hauff, F., Hoernle, K., Schmidt, A., 2003. Sr–Nd–Pb composition of Mesozoic Pacific oceanic crust (site 1149 and 801, ODP Leg 185): implications for alteration of ocean crust and the input into the Izu–Bonin–Mariana subduction system. Geochemistry, Geophysics, and Geosystems 4 (8).

Hofmann, A.W., 1988. Chemical differentiation of the Earth: relationship between mantle, continental crust, and oceanic crust. Earth and Planetary Science Letters 90, 297–314.

Jaillard, E., Ordoñez, O., Suárez, J., Toro, J., Iza, D., Lugo, W., 2004. Stratigraphy of the Late Cretaceous–Paleogene deposits of the Western Cordillera of Central Ecuador: geodynamic implications. Journal of South American Earth Sciences 17, 49–58.

Jaillard, É., Bengtson, P., Ordoñez, M., Vaca, W., Dhondt, A., Suárez, J., Toro, J., 2008. Sedimentary record of latest Cretaceous accretions in Ecuador: the Yunguilla Group in the Cuenca area. Journal of South American Earth Sciences 25, 133–144.

Jaillard, E., Lapierre, H., Ordoñez, M., Toro Álava, J., Amórtegui, A., Vanmelle, J., in press. Accreted oceanic terranes in Ecuador: southern edge of the Caribbean plate? In: James, K., Lorente, M.A. , Pindell, J. (Eds.), Geological Society of London (Special Publication).

Kerr, A.C., Mahoney, J.J., 2007. Oceanic plateaus: problematic plumes, potential paradigms. Chemical Geology 241, 332–353.

Kerr, A.C., Tarney, J., 2005. Tectonic evolution of the Caribbean and north-western South America: the case for accretion of two Late Cretaceous oceanic plateaus. Geological Society of America 33 (4), 269–272.

Kerr, A.C., Tarney, J., Marriner, G.F., Nivia, A., Saunders, A.D., 1997a. The Caribbean–Colombian Cretaceous igneous province: the internal anatomy of an oceanic

plateau. In: Coffin, M.F., Mahoney, J.J. (Eds.), Large Igneous Provinces: Continental, Oceanic and Planetary Flood Volcanism, AGU Geophys. Monograph, vol. 100, pp. 123–144.

Kerr, A.C., Marriner, G.F., Tarney, J., Nivi, A., Saunders, A.D., Thirlwall, M.F., Sinton, C.W., 1997b. Cretaceous basaltic terranes in Western Colombia: elemental, chronological and Sr–Nd isotopic constraints on petrogenesis. Journal of Petrology 38, 677–702.

Kerr, A.C., Aspden, J.A., Tarney, J., Pilatasig, L.F., 2002. The nature and provenance of accreted terranes in Western Ecuador: geochemical and tectonic constraints. Journal of the Geological Society of London 159, 577–594.

Lapierre, H., Dupuis, V., Mercier de Lépinay, B., Tardy, M., Ruiz, J., Maury, R.C., Hernandez, J., Loubet, M., 1997. Is the Lower Duarte Igneous Complex (Hispaniola) a remnant of the Caribbean plume-generated oceanic plateau? Journal of Geology 105, 111–120.

Lapierre, H., Bosch, D., Dupuis, V., Polvé, M., Maury, R.C., Hernandez, J., Monié, P., Yéghicheyan, D., Jaillard, É., Tardy, M., Mercier de Lépinay, B., Mamberti, M., Desmet, A., Keller, F., Sénebier, F., 2000. Multiple Plume events in the genesis of the peri-Caribbean Cretaceous Oceanic Plateau Province. Journal of Geophysical Research 105, 8403–8421.

Lebras, M., Megard, F., Dupuy, C., Dostal, J., 1987. Geochemistry and tectonic setting of pre-collision Cretaceous and Paleogene volcanic rocks of Ecuador. Geological Society of America Bulletin 99, 569–578.

Le Maitre, R.W., Bateman, P., Dudek, A., Keller, J., Lameyre Le Bas, M.J., Sabine, P.A., Schmid, R., Sorensen, H., Steckeisen, A., Woolley, A.R., Zanettin, B., 1989. A Classification of Igneous Rocksand Glossary of Terms. Blakwell, Oxford.

Leterrier, J., Maury, R.C., Thonon, P., Girard, D., Marchal, M., 1982. Clinopyroxene composition as a method of identification of the magmatic affinities of paleo-volcanic series. Earth and Planetary Science Letters 59, 139–154.

Luzieux, L.D.A., Heller, F., Spikings, R.A., Vallejo, C.F., Winkler, W., 2006. Origin and Cretaceous tectonic history of the coastal Ecuadorian forearc between 1°N and 3°S: paleomagnetic, radiometric and fossil evidence. Earth and Planetary Science Letters 249, 3–4, 400-41.

Mamberti, M., 2001. Origin and evolution of two distinct Cretaceous oceanic plateaus accreted in Western Ecuador (South America): petrological, geochemical and isotopic evidence. Thèse de doctorat, Faculté des Sciences de l'Université de Lausanne et de l'Université Joseph Fourier.

Mamberti, M., Lapierre, H., Bosch, D., Ethien, R., Jaillard, É., Hernandez, J., Polvé, M., 2003. Accreted fragments of the Late Cretaceous Caribbean–Colombian Plateau in Ecuador. Lithos 66, 173–199.

Mamberti, M., Lapierre, H., Bosch, D., Jaillard, É., Hernandez, J., Polvé, M., 2004. The Early Cretaceous San Juan plutonic suite, Ecuador: a magma chamber in an Oceanic Plateau. Canadian Journal of Earth Sciences 41, 1237–1258.

McCulloch, M.T., Black, L.P., 1984. Sm–Nd isotopic systematics of Endreby land granulites and evidence for the redistribution of Sm and Nd during metamorphism. Earth and Planetary Science Letters 71, 46–58.

McCulloch, M.T., Chappell, B.W., 1982. Nd isotopic charcteristics of S- and I-type granites. Earth and Planetary Science Letters 58, 51–64.

McCulloch, M.T., Wasserburg, T.H., 1978. Sm–Nd and Rb–Sr chronology of continental crust formation. Science 200 (4345), 1003–1011.

Morimoto, N., Fabres, J., Ferguson, A., Ginzburg, I., Ross, M., Siefert, F., Zussman, J., 1988. Nomenclature of pyroxenes. Bulletin of Minerology 111, 535–550.

Petterson, M.G., Neal, C.R., Mahoney, J.J., Kroenke, L.W., Saunders, A.D., Babbs, T., Duncan, R.A., Tolia, D., McGrail, B., 1997. Structure and deformation of north and central Malaita, Solomon Islands: tectonic implications for the Ontong Java Plateau–Solomon arc collision, and for the fate of coeanic plateaus. Tectonophysics 283, 1–33.

Petterson, M.J., Babbs, T., Neal, C.R., Mahoney, J.J., Saunders, A.D., Duncan, R.A., Tolia, D., Magu, R., Qopoto, C., Mahoa, H., Natogga, D., 1999. Geological-tectonic framework of the Solomon Islands, SW Pacific: crustal accretion and growth within an intra-oceanic setting. Tectonophysics 301 (1–2), 35–36.

Peucat, J.J., Vidal, P., Bernard-Griffiths, J., Condie, K.C., 1988. Sr, Nd and Pb isotopic systematics in the Archean low- to high-grade transition zone of southern India: syn accretion vs. post-accretion granulites. Journal of Geology 97, 537–550.

Pindell, J.L., Kennan, L., Maresch, W.V., Stanek, K.P., Draper, G., Higgs, R. 2005. Plate kinematics and crustal dynamics of circum-Caribbean arc-continent interactions: tectonic controls on basin development in Proto-Caribbean margins. In: Avé Lallemant, H.G., Sisson, V.B. (Eds.), Caribbean–South American plate interactions, Venezuela. Geological Society of America, Special Paper 394, pp. 7–52.

Ramsay, W.R.H., Crawford, A.J., Foden, J.D., 1984. Field setting, mineralogy, chemistry, and genesis of arc picrites, New georgia, Solomon Islands. Contributions to Minerology and Petrology 88, 386–402.

Révillon, S., Arndt, N.T., Hallot, E., Kerr, A.C., Tarney, J., 1999. Petrogenesis of picrites from the Caribbean Plateau and the North Atlantic magmatic province. Lithos 49, 1–21.

Révillon, S., Arndt, N.T., Chauvel, C., Hallot, E., 2000. Geochemical study of ultramafic volcanic and plutonic rocks from Gorgona island, Colombia: the Plumbing system of an oceanic plateau. Journal of Petrology 41, 1127–1153.

Reynaud, C., Jaillard, É., Lapierre, H., Mamberti, M., Mascle, G.H., 1999. Oceanic plateau and island arcs of Southwestern Ecuador: their place in the geodynamic evolution of northwestern South America. Tectonophysics 307, 235–254.

Saunders, A.D., Tarney, J., 1984. Geochemical characteristics of basaltic volcanism within back-arc basins. In: Kokelaar, P.B., Howells, M.F. (Eds.), Marginal Basin Geology, vol. 16. Special Publication of the Geological Society of London, pp. 59–76.

Sinton, C.W., Duncan, R.A., Storey, M., Lewis, J., Estrada, J.J., 1998. An oceanic flood basalt province within the Caribbean plate. Earth and Planetary Science Letters 155, 221–235.

Spikings, R., Winkler, W., Hughes, R.A., Handler, R., 2005. Thermochronology of allochtonous terranes in Ecuador: unraveling the accretionary and post-accretionary history of the Northern Andes. Tectonophysics 399, 195–220.

Sun, S.S., 1980. Lead isotopic study of young volcanic rocks from mid-ocean ridge, ocean islands and island arcs. Philosophical Transactions of the Royal Society of London A297, 409–445.

Thompson, P.M.E., Kempton, P.D., White, R.V., Kerr, A.C., Tarney, J., Saunders, A.D., Fitton, J.G., 2003. Hf–Nd isotope constraints on the origin of the Cretaceous Caribbean plateau and its relationship to the Galapagos plume. Earth and Planetory Science Letters 217, 59–75.

Todt, W., Cliff, R.A., Hanser, A., Hofmann, A.W., 1996. Evaluation of a ^{202}Pb–^{205}Pb double spike for high precision lead isotope analysis. In: Basu, A., Hart, S. (Eds.), Earth Processes: Reading the Isotopic Code. AGU, Washington, DC, pp. 429–437.

Unruh, D.M., Tatsumoto, M., 1986. Lead isotopic composition and Uranium thorium and lead concentrations in sediments and basalts from the Nazca plate. Deep Sea Drill. Project Initial Reports 34, 341–347.

Vallejo, C., Spikings, R.A., Luzieux, L., Winkler, W., Chew, D., Page, L., 2006. The early interaction between the Caribbean Plateau and the NW South American Plate. Terra Nova 18, 264–269.

Vanmelle, J., Vilema, W., Faure-Brac, B., Ordoñez, M., Lapierre, H., Jiménez, N., Jaillard, E., García, M., in press. Pre-collision evolution of the Piñón oceanic terrane of SW Ecuador: stratigraphy and geochemistry of the "Calentura Formation". Bulletin de la Société Géologique de France.

White, W.M., Dupré, B., Vidal, P., 1985. Isotope and trace element geochemistry of sediments from the Barbados Ridge–Demerara Plain region, Atlantic Ocean. Geochim. Cosmochim. Acta 49 (9), 1875–1886.

White, M.W., Albarède, F., Telouk, F., 2000. High-precision analysis of Pb isotopic ratios by multi-collector ICP-MS. Chemical Geology 167, 257–270.

Winchester, J.A., Floyd, P.A., 1976. Geochemical magma type discrimination: application to altered and metamorphosed basic igneous rocks. Earth and Planetary Science Letters 28, 459–469.

Yoneshima, S., Mochizuki, K., Araki, E., Hino, R., Shinohara, M., Suyehiro, K., 2005. Subduction of the Woodlark Basin at the New Britain Trench, Solomon Islands region. Tectonophysics 397, 225–239.

Zindler, A., Hart, S.R., 1986. Chemical geodynamics. Annual Review of Earth and Planetary Sciences 14, 493–571.